Analysis of a delay-differential equation in optical bistability

P. Nardone and Paul Mandel
Université Libre de Bruxelles, Campus Plaine, Code Postal 231, B-1050 Bruxelles, Belgium

Raymond Kapral
Chemical Physics Theory Group, Department of Chemistry, University of Toronto, Toronto, Ontario, Canada M5S 1A1
(Received 24 October 1985)

We study the stability boundaries for the steady and periodic solutions of the Ikeda delay-differential equation. In the limit of an infinite delay the differential equation reduces to a nonlinear map. For this map there exist two classes of boundaries: one corresponding to subharmonic cascades and the other either to domains of bistability for steady or periodic solutions or to the emergence of stable periodic solutions from chaos. For a finite delay we show that each of the above boundaries splits into an infinite sequence of secondary boundaries. The crossing of the secondary boundaries associated with the subharmonic sequence results in the progressive squaring of the periodic solution. The crossing of a secondary boundary of the bistability sequence results in the addition of a frequency in the transient oscillatory relaxation.

I. INTRODUCTION

The purpose of this paper is to study the stability boundaries for the steady and periodic solutions of the Ikeda delay-differential equation[1]

$$G^{-1}dX(t)/dt = -X(t)+a-b\sin[X(t-1)] \qquad (1.1)$$

and to compare them with corresponding boundaries of the map obtained in the singular limit $G\to\infty$,

$$X_t = a - b\sin X_{t-1}\ . \qquad (1.2)$$

Equation (1.1) has appeared in the context of optical bistability. It is by now clear that it provides only an approximate description of an all-optical bistable system. More accurate descriptions require either more nonlinearities and/or higher-dimensional systems of equations.[2-4] However, the sustained interest in Eq. (1.1) stems from two causes. First, there exist a class of hybrid electrooptical bistable devices, which constitute analog-circuit modeling of Eq. (1.1). In this case t is a dimensionless time and G is the dimensionless delay time, which can be controlled either electronically[5-7] or by varying the length of a delay line.[8,9] Recently, an all-optical analog circuit was set up[10] that models Eq. (1.2). The control parameters a and b are proportional to the input voltage, whereas X is the output voltage. Another line of research has focused on acoustooptical devices with similar results.[11-13] Second, Eqs. (1.1) and (1.2) provide fairly simple examples of nonlinear equations that display rich bifurcation diagrams including domains of chaotic dynamics.

The analysis of the map, Eq. (1.2), is straightforward. Although it can be approximated locally by the logistic map for some restricted domains of a and b, it has two basic features that distinguish it from the logistic map: it is a two-parameter, multiple-extremum map. In a recent publication[14] we have shown that a useful global description of the map, Eq. (1.2), is provided by analyzing the stability boundaries of the steady and period-n solutions in the (a,b)-parameter plane. In particular, it was established that besides the subharmonic cascade of period-doubling bifurcations to chaos there is an infinite sequence of bistability domains involving steady, periodic, and chaotic solutions.

The analysis of the reduction of Eq. (1.1) to the discrete map is complicated because $G\to\infty$ is a singular limit. This is best displayed in a calculation by Chow and Mallet-Paret,[15] who analytically constructed the first periodic solution of Eq. (1.1) for large but finite G using the techniques of singular perturbation theory. Results for the solutions of Eq. (1.1) are also provided from an extensive numerical study by Gao *et al.*[16-18] For finite G (including the domain $G<1$), they show that the first infinite subharmonic sequence leading to chaos persists. For the first periodic solution, they relate the transition from a sinusoidal solution to a square-wave solution to an increase in the number of unstable roots in the linear stability analysis. They also report several incommensurate frequencies in the spectrum of the first periodic solution. Finally it was noticed that as G decreases the period of the first periodic solution increases. However, a drawback of these numerical analyses is that very few points in the (a,b)-parameter space have been investigated.

In this paper we show that we can again obtain a global description of Eq. (1.1) by studying the stability boundaries in the (a,b)-parameter plane. A distinct advantage of this procedure is that it relies only on a regular perturbation expansion. This is obvious for the steady solution for which we present a linear and a nonlinear stability analysis. We also show that the relevant properties of the other boundaries can still be derived by approximating the periodic solutions of Eq. (1.1) by the periodic solutions of Eq. (1.2) even for values of G as low as 5. For smaller values of G the general behavior of the boun-

daries remains qualitatively correct but is quantitatively inaccurate.

This paper is organized as follows. In Sec. II we review the properties of the map, Eq. (1.2). We concentrate our analysis on the boundaries of the steady solution and the period-2 solutions. Section III is devoted to a study of the delay-differential equation. In Sec. III A we present a linear stability analysis of the steady solution and describe the boundary striation process which differentiates the map phase diagram from that of the delay-differential equation. In Sec. III B we carry out a nonlinear stability analysis, which is valid in a certain domain. In Sec. III C we study the linear stability of the period-n solutions in the limit of large G. We conclude the paper with a discussion of some general features of this study and comment on the possibility of experimental tests of some of the phenomena.

II. THE DISCRETE MAP

The bifurcation structure of the discrete map, Eq. (1.2), which is obtained from the delay-differential equation in the limit $G\rightarrow\infty$, is easily determined from a linear stability analysis of the periodic solutions. Although only subharmonic and tangent bifurcations are possible for the one-dimensional map, the geometry of their boundaries in the two-parameter (a,b) plane is complex.[14] This one-dimensional map model for the optical bistable device displays the rich variety of phenomena which are exhibited by multiextremum maps governed by two bifurcation parameters.[19–22]

Since the main purpose of this paper is to contrast the behavior of the delay-differential equation (1.1) with the map (1.2), we briefly summarize some of the main features of the bifurcation diagram of the discrete-time map. For our purpose it is sufficient to focus on the bifurcations of the steady state and simple periodic solutions for which analytical results are possible. The fixed points, i.e., the steady solutions $X_t=X$ of the map, are solutions of $X=a-b\sin X$. They become unstable when the slope of the map passes through ±1, $-b\cos X=\pm1$. The lower sign corresponds to a subharmonic bifurcation leading to a period-2 orbit. The boundaries in the (a,b) plane corresponding to this type of bifurcation will be denoted by h_1 (h_n for bifurcation to period n) and are given by

$$a=\pm\arccos(1/b)+b\sin[\pm\arccos(1/b)]+2\pi k\ ,\qquad k=0,1,2,\ldots\ . \tag{2.1}$$

The upper sign in the slope equation corresponds to tangent bifurcation boundaries t_1 (t_n in general for higher periodic solutions), which specify the range of optical bistability for the steady-state solutions. The equations for the t_1 boundaries are

$$a=\pm\arccos(-1/b)+b\sin[\pm\arccos(-1/b)]+2\pi k\ ,\qquad k=0,1,2,\ldots\ . \tag{2.2}$$

Beyond the h_1 boundary we have period-2 solutions of the map,

$$X_1=a-b\sin X_2,\quad X_2=a-b\sin X_1\ . \tag{2.3}$$

A linear stability analysis of this solution indicates that it loses its stability when $b^2\cos(X_1)\cos(X_2)=\pm1$, with the upper and lower signs giving t_2 and h_2 boundaries, respectively. A useful parametric representation of these boundaries is obtained by introducing two auxiliary parameters through $X_1=\sigma-\delta$ and $X_2=\sigma+\delta$. Then we easily find

$$\sigma=2\pi k+\mu_1\arccos[\mu_2\sin\delta/(1-\epsilon\sin^2\delta/\delta^2)^{1/2}]\ ,\qquad k=0,1,2,\ldots \tag{2.4}$$

where $\mu_1^2=\mu_2^2=1$ and $\epsilon=+1$ for t_2 and $\epsilon=-1$ for h_2. In terms of the auxiliary parameters the physical parameters a and b are given by

$$a=\sigma+\delta\tan\sigma/\tan\delta,\quad b=\delta/\cos\sigma\cos\delta\ . \tag{2.5}$$

These h_n and t_n ($n=1,2$) boundaries are shown in Fig. 1. The main features of such a diagram have been discussed earlier.[14] Broadly speaking, as noted above, the subharmonic boundaries, corresponding to a map slope of -1, signal the appearance of a period-doubled orbit. Tangent bifurcations, where the map slope is $+1$, characterize two different kinds of orbit-bifurcation process. First, due to the fact that the map possesses two extrema (in the parameter range of interest), coexistence of orbits of the same and different periods is possible.[20] The birth of a second orbit of the same period can occur through the tangent mechanism and is signaled by the cusps of the tangent boundaries; the number of such cusps in the (a,b) plane doubles as the period of the orbit doubles.[19] Bistability can also arise from the crossing of remote boundary lines. Second, orbits of higher period may also arise by tangent bifurcations out of chaos. Boundaries corresponding to this mechanism are denoted t^*. The t_2^* boundaries are shown in the right-hand portion of Fig. 1.

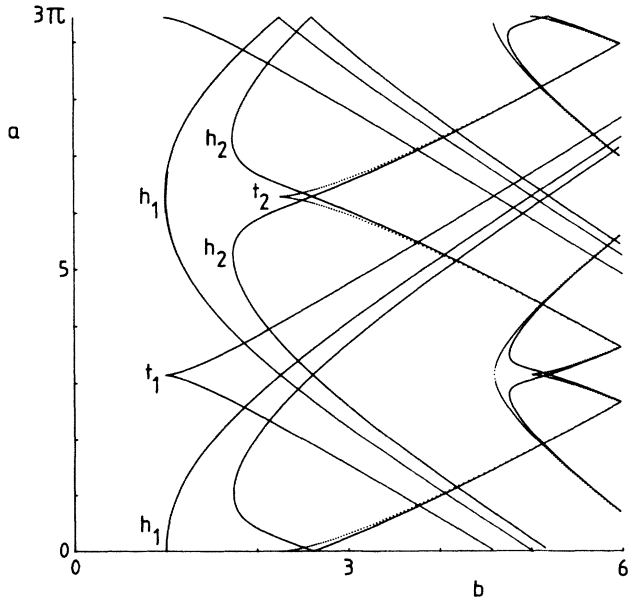

FIG. 1. Harmonic (h_n) and tangent (t_n) boundaries for $n=1$ and 2 in the (a,b)-parameter plane.

Figure 2 displays an enlargement of such a region where both the t_2 boundaries and the t_2^* boundary are shown. From this figure one sees that when the t_2^* boundary is crossed from left to right, a new period-2 orbit is born out of chaos. When the cusp-shaped t_2 boundary is crossed, a second coexisting period-2 orbit is born. The t_2 boundaries shown as dotted lines are extensions of the previously discussed t_2 boundaries. In order to make this structure clear, along the vertical line shown on Fig. 2 at $b=5.2$ we have computed all roots, stable and unstable, of the period-2 solution (2.3). They are shown on Fig. 3. The onset of bistability is clearly evident from the appearance of the sigmoidal regions labeled by c and d in the figure. Once such an orbit is born, its bifurcation history in the parameter plane is analogous to that for steady solutions described above. The entire phase diagram is periodic in a and possesses universal scaling features, which are a generalization of those for a single-extremum, one-parameter map.[20]

We now address the question: To what extent is this structure a faithful description of the delay-differential equation?

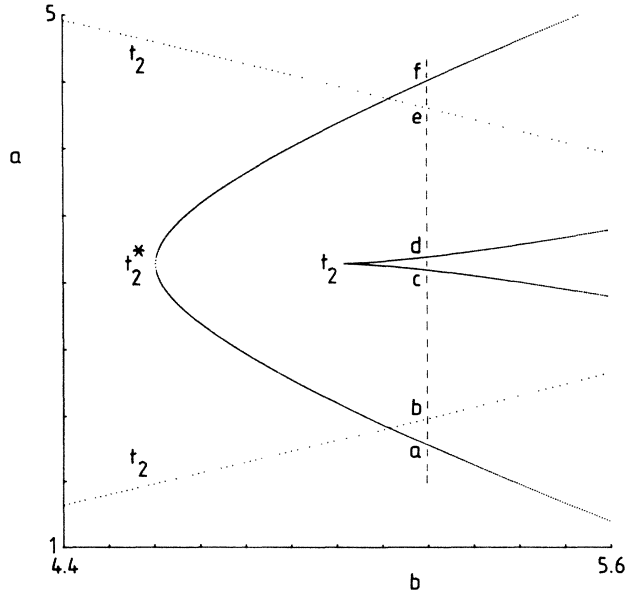

FIG. 2. Enlargement of Fig. 1 showing the t_2 and t_2^* boundaries.

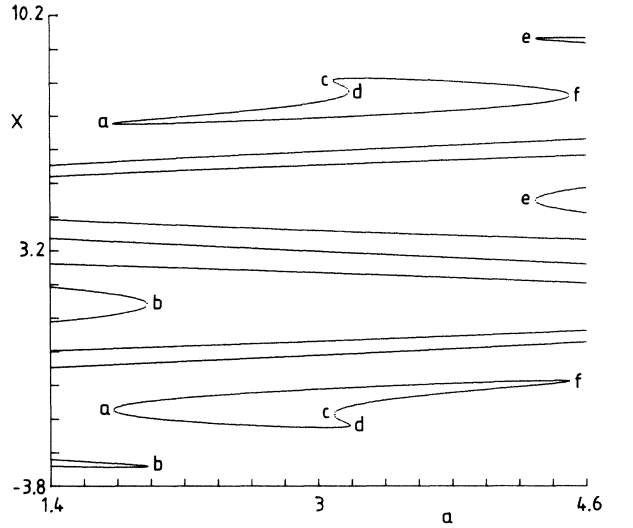

FIG. 3. Stable and unstable period-2 solutions of Eq. (2.3) for $b=5.2$. The letters refer to the crossing of boundaries indicated in Fig. 2.

III. THE DELAY-DIFFERENTIAL EQUATION

A. Linear stability analysis of the steady solutions

The steady solutions of the delay-differential equation (1.1) are independent of G and are given by $X=a-b\sin X$. A linear stability analysis yields the characteristic equation

$$1+be^{-\lambda}\cos X+\lambda/G=0 . \tag{3.1}$$

Letting $\lambda=r+i\omega$, Eq. (3.1) yields

$$G+Gb\cos Xe^{-r}\cos\omega+r=0 ,$$
$$Gb\cos Xe^{-r}\sin\omega-\omega=0 . \tag{3.2}$$

Furthermore, the following relation between r and ω holds:

$$(r+G)^2+\omega^2=(Gbe^{-r}\cos X)^2 . \tag{3.3}$$

When $r>0$ (domain of instability) $|\omega|<Gb$ and the right-hand side of Eq. (3.3) is bounded by $(Gb)^2$. Hence, all unstable roots lie in a circle of radius Gb centered at $r=-G$ and $\omega=0$ in the (r,ω) plane. The portion of the area of this circle which lies in the half-plane $r>0$, A_i, is finite and, therefore, only a finite number of roots of Eq. (3.1) will contribute to the instability of the steady solution. At constant a and b, the area A_i, and therefore the number of roots of Eq. (3.1) that contribute to the instability, varies from zero when $G=0$ to infinity when $1/G=0$. Hence we expect the periodic solution just beyond the bifurcation boundary to vary continuously from a sine function at small G to a square wave at large G. This is just the observed behavior of the solution. We now turn to a more detailed study of the steady-state boundary.

At the stability boundary ($r=0$) we have

$$\tan\omega=-\omega/G , \tag{3.4}$$

$$1+(\omega/G)^2=(b\cos X)^2 . \tag{3.5}$$

A number of interesting features related to the boundary structure can be deduced from the dispersion relation, Eq. (3.4). The root $\omega=0$ corresponds to a unique t_1 boundary. This boundary is independent of G and is identical to that given by Eq. (2.2) for the one-dimensional map. However, in addition to $\omega=0$, the dispersion relation has an infinite number of roots $\omega_j(G)$. They fall into the following two distinct classes:

(1) The odd roots ω_{2j+1} ($j=0,1,2,\ldots$), which vary between $(2j+1/2)\pi$ when $G=0$ and $(2j+1)\pi$ when $G=\infty$.

(2) The even roots ω_{2j} ($j=1,2,\ldots$), which vary between $(2j-1/2)\pi$ when $G=0$ and $2\pi j$ when $G=\infty$.

When $G \geqq 0(1)$, ω_j is numerically indistinguishable from $j\omega_1$.

We first analyze the set of odd roots. To each root ω_{2j+1} there corresponds a boundary h_{1j} whose equation in the (a,b) plane is

$$a=\pm\arccos(z_j/b)+2k\pi+b\sin[\pm\arccos(z_j/b)]\ , \qquad k=0,1,2,\ldots \quad (3.6)$$

with

$$z_j=-[1+(\omega_{2j+1}/G)^2]^{1/2}\ .$$

The first odd root varies between π when $G=\infty$ and $\pi/2$ when $G=0$. Thus, the periodic solution, just beyond the first instability boundary h_{10}, has a period which varies between 2 when $G=\infty$ and 4 when $G=0$. Furthermore, in the limit $G\to\infty$ all odd roots equal π, modulo 2π, and all h_{1j} boundaries collapse into a unique h_1 boundary in this limit. On the basis of the linear stability analysis, one expects that only the first boundary h_{10} will be physically relevant since beyond it the solution is periodic and the next stability boundary will be determined from a stability analysis of this periodic solution. Nevertheless, direct integration of the delay-differential equation has indicated that the h_{1j} boundaries determine important features of the solutions. When the first boundary h_{10} is crossed the steady solution bifurcates to a periodic solution whose frequency is ω_1; this is just a Hopf bifurcation. Upon further variation of a and/or b, a number of h_{1j} boundaries will be crossed before reaching h_{20}. Each time an h_{1j} boundary is crossed the corresponding frequency ω_{2j+1} appears in the power spectrum of the periodic solution with an $O(1)$ weight. This phenomenon is best seen for small G where only a small number of frequencies exist and the distance between two consecutive h_{1j} is maximum. Figure 4 shows a sequence of h_{1j} (and h_{2j} boundaries, see Sec. III C). The periodic solutions of the delay-differential equation and their power spectra are displayed in Fig. 5 for parameter values belonging to Fig. 4. These figures confirm the appearance of the appropriate frequencies as the boundaries are crossed. We note that because Eq. (3.6) derives from a linearized theory the h_{1j} boundaries determined from this equation are only approximate.

The above analysis shows that there are two distinct sequences of h boundaries. There is the principal sequence h_{i0} ($i=1,2,\ldots$) corresponding to bifurcations where the solution doubles its period; this is the only sequence of h boundaries which remains in the $G\to\infty$ limit (discrete map). For finite G there is a secondary sequence h_{ij} ($j>0$), whose relevance has been checked only for the region of the parameter plane lying between h_1 and h_2. Although this secondary sequence is infinite, only a finite number of boundaries are contained between these two curves. The crossing of a secondary boundary results in a "squaring" of the shape of the periodic solution without significant change of its period. As G increases the distance between two consecutive secondary boundaries decreases and in the limit $G\to\infty$ all secondary boundaries coalesce into a single principal boundary. Hence, the first periodic solution has an infinite number of frequencies and may be a square wave.

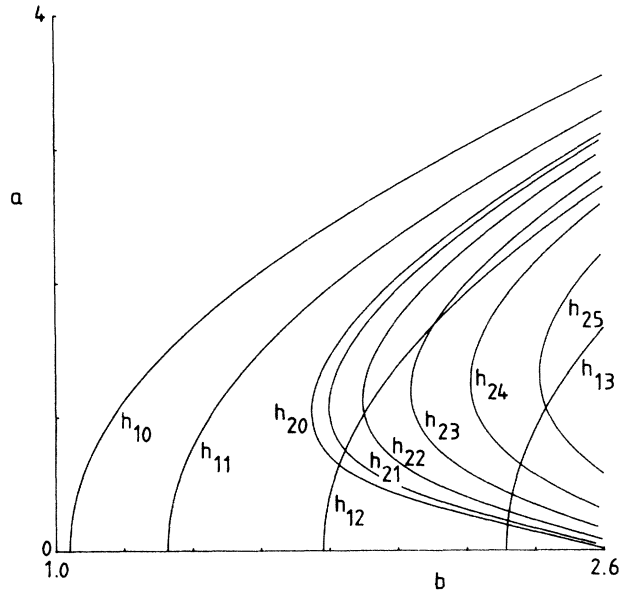

FIG. 4. Striation process of the parameter plane for $G=10$. For clarity, only the secondary boundaries of the first two sequences are shown.

The even roots ω_{2j} of the dispersion relation also yield a set of boundaries, which we label h'_{ij}. The equations determining them are

$$a=\pm\arccos(z_j/b)+2k\pi+b\sin[\pm\arccos(z_j/b)]\ , \qquad k=0,1,2,\ldots \quad (3.7)$$

where

$$z_j=[1+(\omega_{2j}/G)^2]^{1/2}\ .$$

These boundaries lie within the t_1 cusp-shaped boundaries and are tangent to them for large b. They do not have a cusp shape but are similar in form to the harmonic boundaries. We have investigated the role of these boundaries by integration of the delay-differential equation. The crossing of an h'_{ij} boundary has the same effect as the crossing of a secondary h_{ij} boundary, but only on the transient evolution towards the steady state. Crossing of such a boundary introduces an additional even root of Eq. (3.4) in the oscillatory relaxation to the steady state. Again, the boundaries derive from a linear theory and are thus only approximate; the frequency associated with a particular h'_{ij} may appear slightly before the value predicted by Eq. (3.7).

B. Nonlinear stability analysis of the steady solutions

The linear stability analysis of the steady solutions of the delay-differential equation rests on the assumption that there exists a marginally stable solution of the form $X(t)=X+\epsilon\sin(\omega t)$, with $|\epsilon| \ll 1$. In the limit of small G we expect the solutions to be nearly sinusoidal in character and we may instead seek the solutions of the form

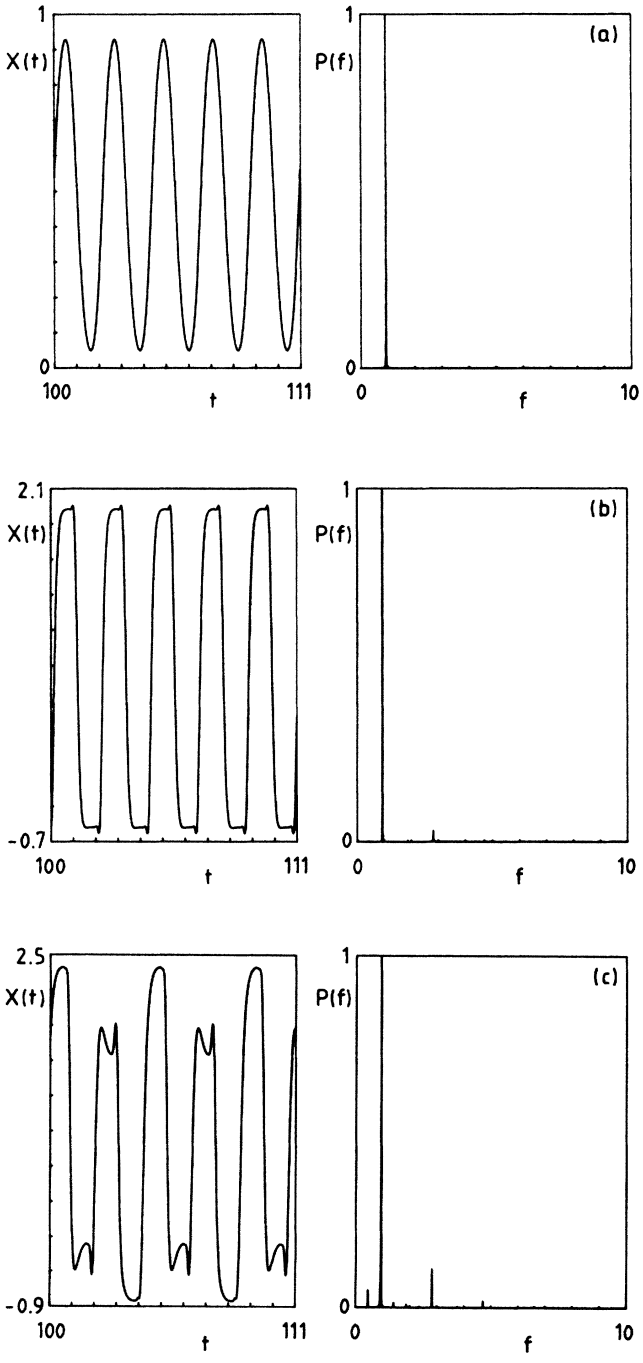

FIG. 5. Periodic solutions and their power spectra for $a=1$, $G=10$. (a) $b=1.2$; initial data, $X(t)=1.2$ for $0\leq t\leq 1$. (b) $b=1.7$; initial data, $X(t)=0.2$ for $0\leq t\leq 1$. (c) $b=1.85$; initial data, $X(t)=0.2$ for $0\leq t\leq 1$.

$$X(t)=X+A\sin(\omega t)+\epsilon R(t),\quad A=O(1) \tag{3.8}$$

where $R(t)$ contains oscillations at all harmonics $n\omega$. Substitution of Eq. (3.8) into Eq. (1.1) and neglecting harmonic terms leads to

$$X=a-bJ_0(A)\sin X\ , \tag{3.9a}$$

$$A\omega G^{-1}\sin\omega=A\cos\omega+2bJ_1(A)\cos X\ , \tag{3.9b}$$

$$\tan\omega=-\omega/G\ , \tag{3.10}$$

where the $J_n(A)$ are Bessel functions of integer order and the third equation is again the dispersion relation Eq. (3.4). Even if we retain the second harmonic contribution in Eq. (3.8) with an $O(1)$ weight, we still recover the same dispersion relation. The new feature brought in by this nonlinear stability analysis is that the coupled equations (3.9) simultaneously determine the mean value X and the amplitude A of the oscillations. We have verified that these results provide a good fit to the numerically determined solutions of the delay-differential equation; they are indistinguishable for small G. The boundary equation, which was given by Eq. (3.5) in the linearized theory, now becomes

$$b\cos X=\pm[1+(\omega/G)^2]^{1/2}A/2J_1(A)\ . \tag{3.11}$$

This result justifies the fact that in the comparison of the linearized theory with the numerical simulations the secondary frequencies were given quite accurately but that the location of the boundaries was only approximate.

C. Linear stability analysis of the square-wave solution

In the limit $G\to\infty$ the striation of the parameter plane by the secondary boundaries becomes dense near the h_n and t_n boundaries and the solutions of Eq. (1.1) approach the square-wave solutions of the map. The period-n solutions of the delay-differential equation may be approximated by

$$X_k=a-b\sin X_{k-1},\quad k=1,2,3,\ldots,n \tag{3.12}$$

in the large-G limit with $X_{k+n}=X_k$. A linear stability analysis of Eq. (3.12) leads to the dispersion relations

$$\tan(\omega+L\pi/n)=-\omega/G,\quad L=0,1,2,\ldots,n-1 \tag{3.13}$$

and to the boundary equation

$$(-b)^n\prod_{k=1}^{n}\cos X_k=\epsilon[1+(\omega/G)^2]^{n/2}\ . \tag{3.14}$$

There are n dispersion relations, each possessing an infinite number of solutions. Let ω_{kn} $(k=0,1,2,\ldots)$ be the roots of Eq. (3.13) with $\omega_{kn}\to(k-L/n)\pi$ when $G\to\infty$. For a given ω_{kn} the boundary equation is given by Eq. (3.14) and will be either an h boundary if $\epsilon=-1$ or a t (or h') boundary if $\epsilon=+1$, with $\epsilon=(-1)^{nk+L}$. Hence the analysis of Sec. III A can be repeated here.

In view of the analysis of Chow and Mallet-Paret, a few comments can be made about the above perturbation calculation around the square-wave solution. Their calculation considers the construction of the boundary layer connecting the two branches of the nearly-square-wave

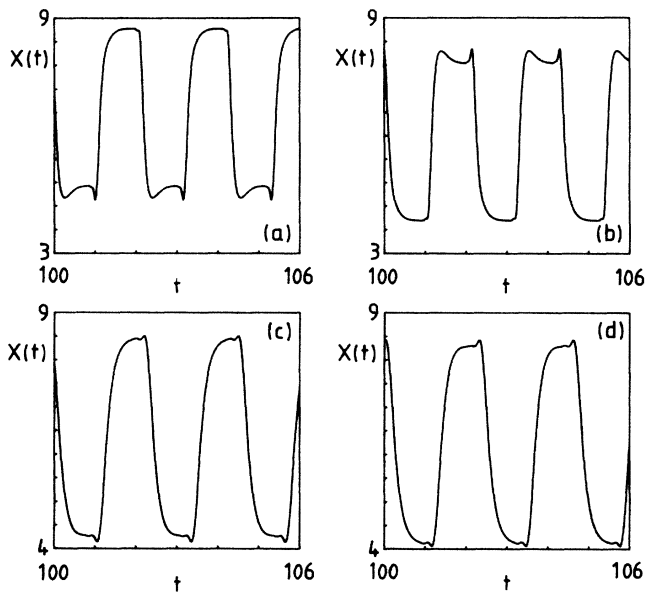

FIG. 6. Bistability for periodic solutions with $a=2\pi$ and $b=2.45$. (a) $G=10$; initial data, $X(t)=4.815$ for $0\leqq t\leqq 1$. (b) $G=10$; initial data, $X(t)=3.780$ for $0\leqq t\leqq$. (c) $G=5$; initial data, $X(t)=4.815$ for $0\leqq t\leqq$. (d) $G=5$; initial data, $X(t)=3.870$ for $0\leqq t\leqq 1$.

periodic solution by singular perturbation techniques for a delay-differential equation with a polynomial nonlinearity. Because of the existence of such a boundary layer, a perturbation calculation of the bifurcation boundaries from the square wave, such as the one we have carried out, is not completely accurate. It assumes that the presence of a thin boundary layer does not significantly affect the boundary location. Explicit numerical calculations for large G confirm that these boundaries constitute a good estimate of the true bifurcation boundaries.

On the basis of the foregoing results we expect the differential equation results to be modeled quite accurately for large G. One feature of the results which is interesting to examine is the character of the bistable states in the cusp regions. Figure 6 shows examples of coexisting solutions in the period-2 cusp for two values of G. These solutions were calculated for parameter values in the center of the cusp and are therefore mirror images of each other. This mirror-image symmetry of the coexisting solutions should make them easy to identify in experiments. We also note that the main features of the bistability persist even to rather small G values where the solutions no longer have a square wave character. The manner in which the bistability disappears for small G is also evident from a comparison of the two figures.

IV. DISCUSSION

The optical bistable device provides an example of a physical system capable of rich dynamical behavior. It can serve as a testing ground for results in nonlinear-dynamical-systems theory. As noted earlier, the delay-differential equation that models such a device in certain situations can be reduced to a discrete-time map model in the $G\rightarrow\infty$ limit. We have already shown that the map-model description of this device shows a much richer structure than the single-extremum one-parameter maps. One of the most noteworthy features is the presence of a hierarchy of bistabilities, which has not yet been observed experimentally. The map model is a member of a class of discrete dynamical systems predicted to display this and other behaviors, but the reduction of the differential equation to the map involves a singular limit. The results of the present study have shown that much of the structure survives for large but finite G.

The bifurcation boundaries for the differential equation can be approximately computed for large G and confirm the predictions of the map model. The analysis of the differential equation has also provided additional results, which are outside the scope of the map model. These include the secondary harmonic boundaries and the structure of the solutions and boundaries for small G, where the solutions are harmonic in character.

The above results suggest a number of experimental tests. Since the cusp bistabilities have been shown to exist for large G, and they have the typically characteristic form shown in Fig. 6, it should not be difficult to search for the low members of the cusp hierarchy since one can determine their location in the parameter plane. These bistabilities should be distinguished from the bistabilities arising from the crossing of remote boundary lines shown in Fig. 1. The other main feature which is susceptible to test is the modification of the power spectra as the secondary harmonic boundaries are crossed. Since the frequencies and the approximate location of the boundaries are known it should be possible to test this feature of the theory.

ACKNOWLEDGMENT

This work was supported in Belgium by the Fonds National de la Recherche Scientifique and the Stimulation Action program of the European Commision, and in Canada by a grant from the Natural Sciences and Engineering Research Council.

[1]K. Ikeda, H. Daido, and O. Akimoto, Phys. Rev. Lett. **45**, 709 (1980).

[2]H. J. Carmichael, R. R. Snapp, and W. C. Schieve, Phys. Rev. **26A**, 3408 (1982).

[3]M. Le Berre, E. Ressayre, A. Tallet, and H. M. Gibbs (unpublished).

[4]S. M. Hammel, C. K. R. T. Jones, and J. V. Moloney, J. Opt. Soc. Am. B **2**, 552 (1985).

[5]H. M. Gibbs, F. A. Hopf, D. L. Kaplan, and R.L. Shoemaker, Phys. Rev. Lett. **46**, 474 (1981).

[6]A. Neyer and E. Voges, IEEE J. Quantum Electron. **QE-18**, 2009 (1982).

[7]P. M. Petersen, J. N. Ravn, and T. Skettup, IEEE J. Quantum Electron. **QE-20**, 690 (1984).
[8]M. Okada and K. Takizawa, IEEE J. Quantum Electron. **QE-17**, 2135 (1981).
[9]M. W. Derstine, H. M. Gibbs, F. A. Hopf, and D. L. Kaplan, Phys. Rev. A **26**, 3720 (1982).
[10]H. Nakatsuka, S. Asaka, H. Itoh, K. Ikeda, and M. Matsuoka, Phys. Rev. Lett. **50**, 109 (1983).
[11]J. Chrostowski, C. Delisle, and R. Tremblay, Can. J. Phys. **61**, 188 (1983).
[12]J. Chrostowski, R. Vallée, and C. Delisle, Can. J. Phys. **61**, 1143 (1983).
[13]R. Vallée and C. Delisle, Phys. Rev. A **31**, 2390 (1985).
[14]P. Mandel and R. Kapral, Opt. Commun. **47**, 151 (1983).
[15]S. N. Chow and J. Mallet-Paret, in *Coupled Nonlinear Oscillators,* edited by J. Chandra and A. C. Scott (North-Holland, Amsterdam, 1983).
[16]J. Y. Gao, J. M. Yuan, and L. M. Narducci, Opt. Commun. **44**, 201 (1983).
[17]J. Y. Gao, L. M. Narducci, L. S. Schulman, M. Squicciarini, and J. M. Yuan, Phys. Rev. A **28**, 2910 (1983).
[18]J. Y. Gao, L. M. Narducci, H. Sadiky, M. Squicciarini, and J. M. Yaun, Phys. Rev. A **30**, 901 (1984).
[19]M. Schell, S. Fraser, and R. Kapral, Phys. Rev. A **28**, 373 (1983).
[20]S. Fraser and R. Kapral, Phys. Rev. A **30**, 1017 (1984).
[21]L. Glass and R. Perez, Phys. Rev. Lett. **48**, 1772 (1982).
[22]J. Belair and L. Glass, Phys. Lett. **96A**, 113 (1983).